

Published in final edited form as:

*Immunity*. 2014 January 16; 40(1): 66–77. doi:10.1016/j.immuni.2013.11.020.

## Transmigrating neutrophils shape the mucosal microenvironment through localized oxygen depletion to influence resolution of inflammation

Eric L Campbell<sup>1,2</sup>, Walter J Bruyninckx<sup>3</sup>, Caleb J Kelly<sup>1,2</sup>, Louise E Glover<sup>1,2</sup>, Eóin N McNamee<sup>1,2</sup>, Brittelle E Bowers<sup>1,2</sup>, Amanda J Bayless<sup>1,2</sup>, Melanie Scully<sup>1,2</sup>, Bejan J Saeedi<sup>1,2</sup>, Lucy Golden-Mason<sup>2</sup>, Stefan F Ehrentauf<sup>1,2</sup>, Valerie F Curtis<sup>1,2</sup>, Adrienne Burgess<sup>1,2</sup>, John F Garvey<sup>4</sup>, Amber Sorensen<sup>2</sup>, Raphael Nemenoff<sup>2</sup>, Paul Jedlicka<sup>2</sup>, Cormac T Taylor<sup>4</sup>, Douglas J Kominsky<sup>1,2</sup>, and Sean P Colgan<sup>1,2</sup>

<sup>1</sup>Mucosal Inflammation Program, Anschutz Medical Campus, Aurora, CO 80045, USA <sup>2</sup>University of Colorado, Anschutz Medical Campus, Aurora, CO 80045, USA <sup>3</sup>Department of Biology, Hanover College, Hanover, IN 47243, USA <sup>4</sup>University College Dublin, Dublin 4, Ireland

### SUMMARY

Acute intestinal inflammation involves early accumulation of neutrophils (PMN) followed by either resolution or progression to chronic inflammation. Based on recent evidence mucosal metabolism influences disease outcomes, we hypothesized that transmigrating PMN influence the transcriptional profile of the surrounding mucosa. Microarray studies revealed a cohort of hypoxia-responsive genes regulated by PMN-epithelial crosstalk. Transmigrating PMN rapidly depleted microenvironmental O<sub>2</sub> sufficiently to stabilize intestinal epithelial cell hypoxia-inducible factor (HIF). Utilizing HIF reporter mice in an acute colitis model, we investigated the relative contribution of PMN and the respiratory burst to “inflammatory hypoxia” in vivo. CGD mice, lacking a respiratory burst, developed accentuated colitis compared to control, with exaggerated PMN infiltration and diminished inflammatory hypoxia. Finally, pharmacological HIF stabilization within the mucosa protected CGD mice from severe colitis. In conclusion, transcriptional imprinting by infiltrating neutrophils modulates the host response to inflammation, via localized O<sub>2</sub> depletion, resulting in microenvironmental hypoxia and effective inflammatory resolution.

### INTRODUCTION

Transmigration of neutrophils (PMN, polymorphonuclear leukocytes) to regions of injury or infection is one of the earliest manifestations of acute inflammation, necessary for host defense. However, without efficient PMN clearance at sites of infiltration, PMN can accumulate and contribute to chronic inflammatory states. Infiltration of PMN is associated with a number of chronic disease states, including ischemic colitis, ulcerative colitis and Crohn’s disease. Energy demanding processes such as migration, phagocytosis and

© 2013 Elsevier Inc. All rights reserved.

Contact: Eric L. Campbell, Ph.D., University of Colorado, Anschutz Medical Campus, 12700 East 19th Ave. Mailstop B-146, Aurora, CO 80045, USA. Phone: 1-303-724-7248; Fax: 1-303-724-7243; eric.campbell@ucdenver.edu.

**Publisher's Disclaimer:** This is a PDF file of an unedited manuscript that has been accepted for publication. As a service to our customers we are providing this early version of the manuscript. The manuscript will undergo copyediting, typesetting, and review of the resulting proof before it is published in its final citable form. Please note that during the production process errors may be discovered which could affect the content, and all legal disclaimers that apply to the journal pertain.

generation of an NADPH oxidase burst accompany infiltration of PMN and are thought to shift the metabolic homeostasis of tissue during inflammation (Kominsky et al., 2010). Considerable advances in understanding the cell-cell interactions that facilitate PMN migration across epithelia have been made (Zen and Parkos, 2003). Relatively little is known, however, about the influence exerted by PMN on surrounding cell types and whether such changes influence tissue function and disease outcome (Colgan et al., 2013a; Colgan et al., 2013b).

In their role within innate immunity, PMN detect and kill invading microbes, through mechanisms involving mobilization of plasma membranes and extrude granule contents (Stie and Jesaitis, 2007). Recruitment of PMN to sites of infection result in killing of invading pathogens via release of granule contents (Amulic et al., 2012), phagocytosis with respiratory burst (Cross and Segal, 2004), release of reactive oxygen or nitrogen species (Radi et al., 1991) and in some instances by generation of extracellular traps (Brinkmann et al., 2004). In this capacity, sites of inflammation tend to become depleted of molecular O<sub>2</sub> (Karhausen et al., 2004). These findings have led to the concept of “inflammatory hypoxia”, in which inflammation and hypoxia are inextricably linked (Colgan and Taylor, 2010). It remains unclear to what extent inflammatory hypoxia impacts the local microenvironment and how such changes might influence disease outcome.

Here we demonstrate mechanisms and outcomes of inflammatory hypoxia *in vitro* and *in vivo* and implicate infiltrating immune cells, principally neutrophils, in shaping the tissue microenvironment through depletion of local molecular O<sub>2</sub>. Guided by global mRNA profiling to ascertain whether PMN “transcriptionally imprint” epithelial cells during transmigration *in vitro*, we hypothesized that PMN-dependent O<sub>2</sub> depletion is integral to regulating inflammatory resolution. Microarray analysis revealed a cohort of hypoxia-responsive genes. Validation studies demonstrated that activated PMN are capable of depleting local O<sub>2</sub> to such an extent that epithelia in close proximity “sense” hypoxia and stabilize the HIF transcriptional machinery. This influence on epithelial HIF activity was dependent on the PMN respiratory burst. Moreover, such localized O<sub>2</sub> depletion proved to be critical for effective mucosal protection and inflammatory resolution.

## RESULTS

### Neutrophil transepithelial migration induces expression of hypoxia-dependent genes

To define the impact of PMN transmigration on the transcriptional profile of intestinal epithelial cells (IECs), we induced PMN to migrate across IECs, harvested RNA and analyzed transcriptional profiles by microarray. Pilot studies involving magnetic bead negative selection involved excessive manipulation, time and resulted in widespread cell death. To minimize alterations in the transcriptional profile due to handling, we adopted a different approach to rapidly obtain representative mRNA. Parallel experiments were performed. First, PMN were induced to transmigrate towards fMLF across polarized monolayers of IECs for 90 minutes, monolayers were washed in fresh medium and after 2hrs RNA was harvested (Figure S1a). Due to the physical interaction of PMN-IECs we termed this “direct” migration. In the second, migration towards fMLF was performed as before, cell-free supernatants were collected following transmigration and applied to naïve IEC monolayers (Figure S1b), after 2hrs RNA was harvested. This model was termed “indirect” due to lack of physical contact between harvested IECs and PMN. In the “direct” experiment, profiling revealed predominantly PMN-specific genes, due to contamination of the monolayer with incompletely migrated neutrophils. In the “indirect” experiment gene regulation induced by physical contact between neutrophils and epithelial cells were lost. However, genes regulated as a result of factors released during transmigration were present. Analyzing genes that were similarly regulated in both experiments enabled us to discern

epithelial-specific regulation of genes in response to activated PMN (Figure 1a). We identified a cohort of hypoxia-regulated genes that were induced in both models in response to PMN (Figure 1b). Gene targets from hypoxia-responsive cluster were validated by qPCR using cDNA from “indirect” transmigration (Figure 1c) and by immunoblot (Figure 1d) using lysates from both “direct” and “indirect” for GLUT1, PGK1 and ADM.

### Activated neutrophils imprint a hypoxic microenvironment into the surrounding tissue

Guided by our findings that PMN transmigration establishes a hypoxic niche, we developed a system to allow for real-time O<sub>2</sub> monitoring. Initial experiments were performed with an Oxylite 2000 probe. Neutrophils were incubated in a hypoxia chamber set at 4% O<sub>2</sub> in the presence of the chemotactic peptide fMLF (N-formyl-methionine-leucine-phenylalanine). A time-dependent depletion of dissolved O<sub>2</sub> was observed (Figure 2a). Given the need for more high-throughput analysis, we adapted a real-time O<sub>2</sub> sensor (SDR, PreSens) where PMN were suspended above the sensor (Figure S1d), which promptly depleted all dissolved O<sub>2</sub>. Utilizing this system we demonstrated that activated PMN rapidly deplete all available O<sub>2</sub> in a cell number- and chemoattractant-dependent manner (Figure 2b).

We sought to ascertain if PMN-mediated O<sub>2</sub> depletion was sufficient for epithelial cells in close proximity to “sense” hypoxia. PMN were suspended in a 0.4μm pore Transwell above T84 intestinal epithelial cells (Figure S1c) in the presence of hypoxia-dependent adduct forming compound (pimonidazole-HCl) dye and activated with fMLF. After 0 minutes (Figure 2c) and 60 minutes (Figure 2d) cells were fixed and localized for hypoxia adducts using Hypoxyprobe-1 antibody. In parallel, examination of epithelial nuclear extracts revealed that PMN transmigration readily stabilized HIF at 3 and 6hr of exposure (Figure 2e). To ascertain if increased nuclear HIF levels resulted in transcriptional activity, HRE-luciferase reporter assays were employed and revealed that incubation of transfected IECs with activated PMN for 3 or 6hr resulted in increased HIF activity as reflected by increased luciferase signal (Figure 2f).

Next we examined the mechanism of O<sub>2</sub> depletion by PMN. Neutrophils were exposed to either vehicle (DMSO) or diphenyleneiodonium (DPI, to inhibit the respiratory burst (Cross and Jones, 1986)) for 15min, washed in PBS and exposed to HRE-Luc transfected IECs. PMN without pre-treatment resulted in an induction of luciferase whereas DPI completely abrogated PMN-mediated stabilization of HIF in adjacent IECs (Figure 2g). These findings strongly implicate the PMN respiratory burst in microenvironmental depletion of molecular O<sub>2</sub>.

Mice lacking functional NADPH oxidase in PMN (*Nox2*<sup>-/-</sup>, or CGD mice) phenotypically mirror human chronic granulomatous disease (CGD), due to a deficiency in PMN respiratory burst activity (Dinauer et al., 1987). To define the contribution of the respiratory burst in O<sub>2</sub> depletion, we harvested bone marrow PMN from both wild-type C57/B6 and CGD mice, incubated with/without DPI for 15min on ice and tracked consumption of dissolved utilizing a novel real-time O<sub>2</sub> sensor (Figure S2). As proof-of-principle, PMN from phorbol myristate acetate (PMA) activated wild-type mice increased luciferase activity in HRE-transfected epithelia, and this influence was abrogated with DPI. Moreover, CGD PMN were incapable of inducing epithelial hypoxia (Figure 2h) in the presence or absence of DPI. Taken together, these data demonstrate that PMN deplete sufficient O<sub>2</sub> to render nearby IECs hypoxic, via the NADPH oxidase burst.

## Neutrophil infiltration establishes a hypoxic microenvironment during acute colonic inflammation

To recapitulate our findings *in vivo*, we utilized the trinitrobenzenesulfonic acid (TNBS) colitis model of murine acute colonic inflammation. Chemically-induced models of colitis are frequently criticized for not accurately recapitulating ulcerative colitis in humans, a chronic inflammatory condition complicated by defects of both innate and adaptive immunity (Khor et al., 2011) and are considered merely models of acute colonic inflammation. We elected to use TNBS over other acute models of colonic inflammation due to its early potent recruitment of PMN (maximal at 12 – 24hr). Unlike the dextran sulfate sodium model, which relies on denuding epithelia to expose the mucosa to luminal contents, which makes investigation of PMN-epithelial interactions difficult. Finally, TNBS is a self-resolving acute inflammation making it an ideal model to study PMN-epithelial interactions in the context of colonic inflammation (Van Rees et al., 1997). Utilizing HIF reporter ODD-luc mice (Safran et al., 2006) in combination with whole tissue imaging, we quantified induction of colonic inflammation-associated hypoxia (Figures 3a and 3b). Maximal luciferase expression in colitis was observed in the cecum (Figure 3a) and was patchy throughout the colon of colitic animals.

To define the role of PMN in tissue hypoxia during colitis, we depleted PMN using Gr-1 in ODD-luc mice (Kuhl et al., 2007) and elected to harvest after 2 days to capture tissue changes occurring before clearance of PMN by macrophages. Flow cytometry indicated a >90% depletion of circulating PMN with Gr-1 (91.63% in vehicle and 97.47% in TNBS), with minimal influence on circulating monocyte numbers (Figure S3). TNBS administration resulted in marked weight loss on days 1 and 2 (Figure 3c). Depletion of PMN during colitis resulted in ultimately more severe weight loss on day 2 (Figure 3c). A trend towards colon shortening occurred with TNBS, however, with PMN depletion greater colon shortening was observed (Figure 3d). Tissue myeloperoxidase (MPO) measurements were performed to quantify PMN influx and demonstrated a reduced number of tissue PMN during colitis (Figure 3e). Multiplex ELISAs revealed increases of tissue cytokines for IL-1 $\beta$  and IL-12/p70 in TNBS, which was abrogated by Gr-1 depletion of PMN. Additionally, increases in tissue IFN- $\gamma$  and mKC were observed in TNBS but levels were amplified by PMN depletion (Figure 3f). Tissue HIF-dependent luciferase activity was abrogated by Gr-1-mediated PMN depletion (Figure 3g). Histologic examination revealed a prominent granulocytic infiltrate in TNBS mice coupled with severe mucosal damage (Figure 3h middle panel), consistent with clinical parameters of weight loss and colon shortening (Figures 3c and d). PMN depletion aggravated the mucosal damage, wherein infiltrating leukocytes were non-PMN cell types (Figure 3h right panel), consistent with previous findings that PMN depletion significantly enhances inflammation in colitis in rats (Kuhl et al., 2007). Immunohistochemical staining for hypoxia-dependent firefly luciferase (green) and neutrophil-specific marker Ly6g (red) indicated a concomitant induction of luciferase in regions of neutrophil infiltration in TNBS (Figure 3i middle panel) relative to vehicle treated mice (Figure 3i left panel) or in TNBS with Gr-1 mediated PMN depletion (Figure 3i right panel). Taken together, such findings substantiate our *in vitro* results that infiltrating PMN deplete local O<sub>2</sub> amounts and that ensuing hypoxia influences the severity of the inflammatory response.

## Evidence of microenvironmental hypoxia in crypt abscesses

We extended these findings to humans and identified biopsies from patients with ulcerative colitis that showed active disease with crypt abscess formation. Serial sections were stained for H&E and immunohistochemical detection of the HIF target Glut1. As shown in Figure 4, tissue margins revealed healthy crypts (Figure 4a) and low expression of Glut1 (Figure 4b). In stark contrast, regions of tissue with active crypt abscesses (Figure 4d) revealed prominent parallel localization of PMN and robust staining for Glut1 (Figure 4e). Higher

magnification of control (Figure 4c) and colitis (Figure 4f) revealed de novo staining surrounding transmigrating PMN (inset, Figure 4f). Colonic biopsies from un-inflamed (Figure 4g) and HIV patients (Figure 4h) with marked T-cell infiltration but few neutrophils were stained as an inflammatory disease control to demonstrate specificity of tissue hypoxic responses to PMN. Quantification of image intensities illustrates PMN (Figure 4i) and Glut1 (Figure 4j) staining. Thus, inflammatory hypoxia occurs in vivo and is specific for inflammatory lesions associated with PMN influx.

### **Mice lacking respiratory burst exhibit defective inflammatory resolution**

To specifically delineate the influence of the PMN respiratory burst in the establishment of a hypoxic microenvironment during colitis, we attempted to induce colitis in the CGD mice. In these mice, TNBS elicited a response so prominent that few animals survived (Figure 5a). A dose response with various concentrations of TNBS and vehicle carrier (ethanol) identified conditions that permitted the study of colitis without excessive attrition (Figure 5b). In wild-type mice, peak disease usually occurs on day 2, with resolution beginning on day 3. Based on weight loss curves (Figure 5c) and colon length (Figure 5d), the lack of a respiratory burst appeared to impede the resolution phase of disease. Such findings were not a result of failure of PMN to migrate to the tissue, evidenced by myeloperoxidase activity (Figure 5g). Indeed, histologic examination of these tissues revealed prominent increase in PMN within the colonic submucosa of CGD mice (Figure 5e), which may indicate delayed or failed resolution. In Figure 5f, sections were stained with Hypoxyprobe-1. Vehicle-treated wild-type and CGD mice displayed prominent luminal epithelial staining, indicated by white arrowheads. TNBS resulted in extensive Hypoxyprobe-1 staining, permeating deep into the crypt structure, indicated by yellow arrowheads. Concomitant with increased PMN infiltration, the CGD mice had an appreciable lack of Hypoxyprobe-1 staining within the mucosa. Most striking was the apparent lack of luminal epithelial staining. Notable were regions with what appear to be bacteria deep in crypt lumen, wherein the epithelium responded with positive Hypoxyprobe-1 staining (white arrows). Enrichment of epithelial cells followed by RNA isolation and qPCR revealed increased expression of PGK1 and Glut1 transcripts in TNBS-treated wild-type, which were not induced in CGD mice (Figure 5h).

To quantify the relative contribution of the respiratory burst to hypoxia in colitis, we bred a first-generation cross of CGD mice with the ODD-luc mice (CGDx) and a control C57/B6 crossed to ODD-luc (B6x) see (Figure S4) for breeding strategy. As *Nox2* is X-linked, mating female CGD mice with ODD-luc males resulted in a progeny that was either hemizygous for the CGD phenotype (females) or homozygous (males). Bone marrow-derived PMN from the control cross (B6x) consumed O<sub>2</sub> rapidly in response to PMA-stimulation; however, male CGDx mice did not deplete O<sub>2</sub> in response to activation. Hemizygous female CGDx did deplete O<sub>2</sub>, but at a slower rate to the B6x mice (Figure 5i). Moreover, tissue luciferase levels from B6x mice reaffirm the finding that TNBS induces tissue hypoxia (Figure 5j) since male CGDx mice were unable to generate a hypoxic microenvironment in response to TNBS, as measured by tissue luciferase (Figure 5j). These findings demonstrate that CGD mice develop severe non-resolving colonic inflammation coupled with a failure to elicit mucosal hypoxia.

### **Mucosal HIF stabilization ameliorates colitis severity in mice lacking respiratory burst**

Our previous work demonstrated that pharmacological HIF stabilization is protective in mucosal inflammation in wild-type mice (Robinson et al., 2008). Coupled with these findings, we consequently proposed that the severity of colitis in CGD mice was due to a lack of hypoxic signaling within the mucosa. We examined whether pharmacological intervention could restore normal hypoxic signaling, recapitulate the wild-type inflammatory



hypoxic microenvironment within the mucosa and attenuate the severity of colitis in the CGD mice. To accomplish in vivo HIF stabilization, both wild-type and CGD mice were administered the PHD inhibitor (HIF stabilizer) AKB-4924 (Okumura et al., 2012). In wild-type mice, TNBS administration with sham injection resulted in weight loss (Figure 6a top panel,  $p < 0.001$  compared with vehicle on days 1–4 by two-way ANOVA). AKB-4924 administration was protective as reflected by decreased weight loss ( $p < 0.001$  compared with TNBS alone on days 2–4;  $p > 0.05$  compared with vehicle + AKB-4924 on days 2–3) and a more rapid return to normal body weight. In the CGD mice TNBS elicited severe weight loss (Figure 6a bottom panel,  $p < 0.001$  compared with CGD vehicle on days 1–4). By day 3 TNBS-treated wild-type mice regained weight, which was not evident in CGD mice ( $p < 0.05$  CGD versus WT + TNBS on day 3). While an improvement was observed in the CGD mice with AKB-4924 administration ( $p < 0.05$  on day 1;  $p < 0.01$  on day 2;  $p < 0.001$  on day 3–4), there remained a significant difference between the vehicle-treated and the AKB-4924 treated CGD mice ( $p < 0.001$ ). In fact, AKB-4924 administration during colitis to CGD mice more closely resembled wild-type mice with TNBS ( $p > 0.05$  by two-way ANOVA).

AKB-4924 administration resulted in protection against colon shortening in both wild-type and CGD mice (Figures S5a & S5b). Histological scoring revealed increases in both inflammatory score and injury score of wild type and CGD mice following TNBS administration (Figure 6b). While no significant differences were observed in the overall inflammatory score between wild-type and CGD-TNBS treatments without AKB-4924, CGD mice exposed to TNBS without AKB-4924 demonstrated higher injury scores. Moreover, AKB-4924 attenuated both inflammatory and injury scores. These findings were also evident by H&E (Figure 6e, top panel; see also Figure S6a).

Colon tissues were processed for flow cytometry to determine the extent of infiltration of various cell types. TNBS resulted in increased recruitment of CD45<sup>+</sup> cells to the colon in both wild type and CGD mice. Interestingly, in CGD mice, the increase in CD45<sup>+</sup> cells appeared to be predominantly neutrophils and monocytes, both of which were abrogated by AKB-4924 administration (Figure 6c, see also Figure S5c). No appreciable differences in total CD3<sup>+</sup> T-cell numbers were observed.

Tissue cytokines were assayed and revealed trends towards increased pro-inflammatory cytokines (IL-1 $\beta$ , IFN- $\gamma$ , mKC, and IL-12) in both wild-type and CGD mice during TNBS that were largely abrogated by AKB-4924. Furthermore mucosal protective cytokines (IL-6 and IL-10) levels were enhanced by HIF stabilization (Figure 6d). Considering the role of bioactive lipids in resolution of acute inflammation (Serhan and Chiang, 2013) and our previous findings demonstrating resolution of colitis with pro-resolving lipids (Campbell et al., 2010), we assessed the influence of TNBS and AKB-4924 treatment on the generation of pro-resolving lipids, including Resolvin D1 (RvD1) and 15-epi-Lipoxin A4 (Figure S5d). Tissue ELISAs revealed increased local RvD1 generation, following TNBS treatment in wild-type and a decrease in CGD mice. Significant increases in RvD1 were observed following AKB-4924 treatment in both wild-type ( $p < 0.001$ ) and CGD ( $p < 0.05$ ) mice. Similarly, trends towards increased 15-epi-LXA4 were detected in TNBS-treated wild-type mice and decreased levels in CGD. A significant increase was detected in wild-type mice following treatment with the PHD inhibitor ( $p < 0.05$ ). To rationalize these finding we investigated expression of PTGS2 (cyclooxygenase-2), an enzyme involved in the de novo generation of both of these lipids and a known hypoxia-dependent gene. We detected a trend towards increased PTGS2 transcript in wild-type mice following TNBS treatment and in AKB-4924-treated colitic mice (Figure S5e) and increases in expression in CGD following PHD inhibition.

Immunohistochemical staining for Hypoxyprobe-1 (Figure S6b) indicated enhanced tissue hypoxia in wild-type mice following TNBS administration, however this was absent in CGD mice. These disparate phenotypes were both abrogated by AKB-4924 treatment. Sections were also stained for HIF-1 $\alpha$  in CGD (Figure 6e, bottom panel) and wild-type (Figure S6c), which revealed both enhanced HIF-1 $\alpha$  staining (Figure 6f) and co-localization of HIF-1 $\alpha$  with nuclei in colonic crypts following AKB-4924 administration (indicated by yellow arrow heads and quantified in Figure 6g), demonstrating that AKB-4924 mediated HIF-1 $\alpha$  stabilization within the mucosa. Taken together, these studies reveal that the innate immune deficit of CGD mice can be overcome by PHD inhibition within the colonic mucosa.

### **Mucosal HIF stabilization enhances barrier function by increasing goblet cell number**

We elected to focus on the apparent infiltration of bacteria in the colonic crypts of CGD mice during colitis utilizing fluorescent *in situ* hybridization (FISH) with a ubiquitous Eubacterial probe. In both CGD (Figure 7a) and wild type (Figure S7a) vehicle-treated mice bacteria associate with luminal epithelia. There was no indication of bacterial invasion into the mucosa. Upon exposure to TNBS, bacteria were observed to invade deep into the crypts of CGD but not wild-type (Figure S7a). Conversely, in PHD-inhibited mice, bacteria were not observed to interact with epithelia and a clear margin was observed. To determine if these bacteria disseminate past the mucosa, we aseptically removed mesenteric lymph nodes (MLN) and harvested blood by cardiac puncture. Bacterial dissemination was quantified by qPCR for 16S rDNA in MLN (Figure 7b) and serum LPS measurements (Figure 7c), both indicating an increased bacterial load in CGD mice following TNBS treatment, prevented by pre-treatment with AKB-4924.

To investigate if the decreased bacterial infiltration was mitigated via altered epithelial barrier function, we examined mucus production by Alcian blue staining in CGD mice (Figure 7d) and in wild-type (Figure S7b). More intense staining of goblet cells were observed and quantification of goblet cell numbers per crypt (Figure 7e) revealed an increase following PHD inhibition. Concordantly epithelial barrier permeability was determined by assaying serum fluorescence following FITC-dextran gavage (Figure 7f). We conducted qPCR from enriched epithelial isolates for known HIF-dependent barrier protective genes that modulate the mucus layer: *Muc3* (Louis et al., 2006) and *Tff3* (Furuta et al., 2001), were both induced by AKB-4924 PHD inhibition (Figure 7g). Such results implicate a prominent induction of mucin and mucin-binding elements by PHD inhibition.

## **DISCUSSION**

“Inflammatory-hypoxia” (Karhausen et al., 2004) is thought to result from numerous factors including increased metabolic demand and decreased O<sub>2</sub> delivery (Colgan and Taylor, 2010). Here, we demonstrate that actively migrating PMN establish a microenvironment permitting surrounding tissues to “sense” O<sub>2</sub> depletion. Epithelial cells left in the wake of migrating PMN become transcriptionally imprinted, displaying a prominent hypoxic signature. By utilizing both a “direct” and “indirect” transmigration model and examining genes regulated similarly in both, we were able to exclude the potential for PMN gene contamination. Our *in vitro* real-time oxygen sensing experiments demonstrate the extent of oxygen depletion in media post-PMN activation, despite continuous mixing. Incubation of epithelia with “indirect” supernatants also resulted in HIF stabilization, which we attributed simply to oxygen depletion. Although we cannot outright exclude other mechanisms, for instance epithelial-derived exosomes (Bobrie et al., 2012), PMN-derived microparticles (Dalli and Serhan, 2012; Lim et al., 2013) effecting intercellular genetic communication via microRNAs (Mittelbrunn and Sanchez-Madrid, 2012) or adenosine-mediated non-oxygen related signaling pathways such as deneddylation of Cul-2-containing RING ligases

(Ehrentraut et al., 2013) leading to HIF-1 $\alpha$  stabilization in normal oxygen tensions; ultimately the endpoint is epithelial HIF signaling.

Given the protective nature of HIF in the mucosa, such findings reveal a previously unappreciated molecular mechanism for PMN-mediated resolution of inflammation. Likewise, NF $\kappa$ B has been demonstrated to be anti-apoptotic in intestinal epithelia and is protective in murine models of colitis (Chen et al., 2003). The stabilization and activity of both NF $\kappa$ B and HIF $\alpha$  subunits are regulated by the O<sub>2</sub>-dependent PHDs (prolyl hydroxylases). Inhibition of PHDs results in enhanced HIF and NF $\kappa$ B activity and has been implicated as mucosal-protective in both DSS (Cummins et al., 2008) and TNBS (Robinson et al., 2008) models of colitis.

ODD-Luciferase mice permitted quantification of inflammatory hypoxia in experimental colitis. Consistent with previous work (Karhausen et al., 2004), this analysis revealed prominent stabilization of HIF in both the cecum and in patchy regions along the wall of the colonic mucosa. Patient samples mirrored this finding, revealing concomitant staining of HIF-target Glut-1 in epithelia surrounding crypt abscesses. Antibody-mediated depletion of murine PMN indicated that PMN fundamentally contribute to the establishment of the hypoxic microenvironment evident during acute inflammation. Consistent with previous work in rats (Kuhl et al., 2007), PMN depletion exacerbated colitis, suggesting that stabilization of HIF, by infiltrating PMN in the present work, promotes a protective phenotype within the mucosa.

Mechanistically, PMN-mediated tissue hypoxia required a functional respiratory burst, mediated via the PMN NADPH oxidase complex (Nauseef, 2008). Use of the flavoprotein inhibitor DPI and CGD mice implicated NADPH oxidase in O<sub>2</sub> depletion and stabilization of HIF in adjacent epithelia. Murine CGD PMN were incapable of generating a hypoxic microenvironment or stabilizing epithelial HIF. Of interest in this regard, it is recognized that a subset of CGD patients develop colonic inflammation (Huang et al., 2004). Consistent with this clinical observation, CGD mice developed a severe colitic phenotype. While the epithelium remained relatively intact in wild type mice with TNBS, severe damage to the mucosa occurred, accompanied by a lack of discernible pimonidazole adduct localization in CGD mice and a greater influx of PMN. Likewise, our results demonstrated that HIF stabilizers (PHD inhibitors) are sufficient to provide mucosal protection and abrogate the CGD phenotype.

Neutrophil numbers decrease during resolution of TNBS colitis due to clearance by macrophages (Cox et al., 1995; Savill et al., 1989). In the CGD mice neutrophil and macrophage numbers are increased in the absence of a respiratory burst, potentially indicative of failed clearance (Sanmun et al., 2009). PHD inhibition was protective against the CGD colitis phenotype, restoring PMN and monocyte levels to normal, concomitant with enhanced tissue protection and mucosal HIF stabilization. Whereas the PHD inhibitor AKB-4924 has been recently demonstrated to augment the antimicrobial activity of PMN independent of the respiratory burst (Okumura et al., 2012), our studies demonstrate diminished bacterial translocation due to enhanced mucosal barrier function, which likely has a greater impact in the CGD mice. Identification of bacteria deep in the colonic crypts of CGD mice following colitis, coupled with aberrant goblet cell distribution throughout the crypts that was reversible with PHD inhibition, suggested that AKB-4924 may influence goblet cell survival or function. Adherent and fluid mucus layers, secreted by goblet cells, limit physical interaction with luminal bacteria (Johansson et al., 2011). Impaired goblet cell function or mucus layer forming proteins (Muc2, Tff3) have been implicated in the pathogenesis of chronic colonic inflammation (Beck et al., 2010; Van der Sluis et al., 2006). We examined murine epithelial *Muc3* and *Tff3*, known HIF-dependent gene products, as a



proof-of-principle and demonstration that colonic mucus was being affected. HIF has been implicated in goblet cell hyperplasia in the lung (Polosukhin et al., 2011). Moreover, *Tff3* expression has been implicated in limiting epithelial apoptosis (Taupin et al., 2000) and promoting mucosal healing (Mashimo et al., 1996), possibly via induction of IL-6 (Taupin and Podolsky, 2003). Considering the sheer plethora of potential innate and adaptive deficiencies potentially associated with chronic inflammatory conditions like ulcerative colitis (Khor et al., 2011), it is unclear if PHD inhibition could provide a viable therapeutic option. However, as mentioned previously the innate deficit in CGD patients often leads to severe chronic colonic inflammation similar to ulcerative colitis (Huang et al., 2004).

Taken together, these results provide new molecular insight into the role of PMN in inflammatory resolution. Transcriptional imprinting of select signaling pathways, exemplified here by HIF, provides mucosal memory after the clearance of PMN and elicits functional resolution responses important to tissue homeostasis. Although PMN accumulation in crypt abscesses is a hallmark of mucosal inflammation, our findings suggest that PMN infiltration is a necessity for limiting disease severity. Our studies show that the respiratory burst is fundamental for initiating a hypoxic microenvironment, impeding further PMN infiltration and restoring hypoxic signaling to the mucosa is sufficient to overcome the resolution deficit (e.g. in CGD mice). These findings demonstrate the beneficial impact and regulatory influence of PMN-mediated HIF stabilization within discrete regions of the mucosa and provide important insight into therapeutic options for inflammatory mucosal disease.

## EXPERIMENTAL PROCEDURES

### Materials and Methods

IECs were cultured and transfected as described previously (Campbell et al. 2010). Caco-2 were used for transfections, T84 were used for all other in vitro experiments. HIF-1 $\alpha$  and tissue cytokines were quantified by Mesoscale (MSD). PHD inhibitor (AKB-4924) was provided by Akebia Pharmaceuticals.

### Neutrophil-epithelial interaction models

Neutrophils were subjected to either “Direct” transmigration, “Indirect” transmigration, “Co-culture” or “SDR real-time O<sub>2</sub>” models (Figure S1). For “Direct” transmigration T84 IECs were grown to confluence (TER > 2,000  $\Omega \cdot \text{cm}^2$ ) on the underside of collagen-coated Transwell 5.0 $\mu\text{m}$  pore permeable supports (Corning). A chemotactic agent (1 $\mu\text{M}$  fMLF in HBSS) was applied to the apical surface (bottom chamber). Neutrophils ( $1 \times 10^6$ ) were applied to the basolateral side (top) to allow transmigration in the physiologically relevant basolateral-apical direction. In the “Indirect” model, conditioned supernatants from “Direct” transmigration were collected, clarified by centrifugation (350 $\times g$  for 10min) and applied to naive T84 monolayers. In the “Co-culture” model, epithelial cells were cultured in 24-well plates. PMN were suspended above them using permeable supports that prevented physical interaction between PMN and epithelia (0.4 $\mu\text{m}$  pore).

### O<sub>2</sub> Measurements

Initial pO<sub>2</sub> experiments were carried out with an Oxylite 2000 probe (Oxford Optronix, UK). Measurements were performed at 4% O<sub>2</sub> in a hypoxia chamber. Subsequent real-time O<sub>2</sub> measurements were made with Oxodish plates on an SDR reader (PreSens) and performed in normoxia. Oxodish 24-well plates were pre-equilibrated with HBSS+ or HBSS + containing either fMLF or PMA. Transwell filters (Corning; 0.4 $\mu\text{m}$  pore) were suspended above the O<sub>2</sub> sensor to physically separate PMN from the sensor. Freshly isolated

neutrophils from either whole venous blood of healthy volunteers or mouse bone-marrow derived PMN were applied to the filter.

### Microarray and analysis

Cyanine-3 (Cy3) labeled cRNA was prepared from 0.2 µg total RNA using the One-Color Quick Amp Labeling kit (Agilent) according to the manufacturer's instructions, followed by RNeasy column purification (Qiagen). Cy3-labelled cRNA and hybridized to Agilent 4×44K human whole-genome arrays. Data was analyzed using GeneSpring GX12 (Agilent Technologies) and deposited in the NCBI GEO database (accession number: GSE39681).

### Patient samples and Histological scoring

Sections from archived biopsy tissue from IBD patients were obtained using approved human research protocols from the Colorado Multi-Institutional Review Board and screened for presence of active disease with crypt abscesses. Histological assessment was performed by a pathologist (PJ), blinded to strain and treatment groups. The following standardized semi-quantitative system scores were applied for the following parameters: (1) active inflammation (granulocyte infiltration); (2) chronic inflammation (lymphocytes and macrophages in the mucosa and submucosa); and (3) colonic gland distortion. Biopsy samples with crypt abscesses were used for immunohistochemical analysis.

### Mice and chemically-induced colitis

Wild-type (C57/B6), CGD (*Nox2*<sup>-/-</sup>) and ODD-luciferase mice were purchased from Jackson laboratories. Mice were housed in ventilated cages. One week prior to induction of colitis, mice were pre-sensitized by skin painting with 1% TNBS in 80% EtOH. On day 0, mice were anesthetized and received a 100µl rectal instillation of either vehicle (50% EtOH) or TNBS (2.5% TNBS in 50% EtOH). For neutrophil depletion, mice were injected with either 1mg/kg i.p. of Gr-1 or sham (isotype control rat IgG2b), on days -1 and day 0, prior to TNBS rectal instillation. Daily treatment with 5mg/kg either AKB-4924 or vehicle (carboxymethylcellulose) by i.p. injection occurred on days -1 through day 2. Colons were removed from ODD-Luciferase mice post-TNBS administration for bioluminescent imaging using an IVIS Imaging System 50 Series (Caliper Life Sciences/Xenogen Corp). Animal protocols were approved by the Institutional Animal Care and Use Committee at the University of Colorado.

### Epithelial enrichment, immune cell isolation and flow cytometry

For demonstration of granulocyte depletion, whole blood was collected from anaesthetized animals by cardiac puncture and anticoagulated with K2-EDTA.

Mouse colonic sections were prepared by removal of the epithelium in HBSS- with 5mM EDTA. Following agitation, liberated epithelia were removed by passing through a 70µm pore filter. Remaining tissue was digested for immune cell isolation. Flow-through epithelia were washed in HBSS- and purified by immunomagnetic negative selection using the EasySep Mouse epithelial cell enrichment kit (Stemcell Technologies) as directed by manufacturer. Recovered epithelia were immediately processed for RNA isolation.

Remaining tissue was digested at 37°C, for 15min with agitation in digestion buffer [1mg/ml Collagenase (Sigma), 0.5mg/ml Dispase (Gibco), 0.1mg/ml DNase I (Sigma) in RPMI 1640 (HyClone) with 1% FBS (Gibco)] and subsequently neutralized with an equal volume of cold complete medium. Debris was removed by decanting through 70 µm pore mesh filter. Cells were pelleted and resuspended in FACS buffer (5% FBS, 1% BSA, 0.1% NaN<sub>3</sub> in PBS).

Cells were incubated with fluorescently labeled antibodies against mouse CD45 (30-F11) MHC class II (M5/114.15.2), CD11c (N418), Ly6c (HK1.4) (eBioscience), CD11b (M1/70), Ly6g (1A8) and SiglecF (E50-2440) (BD Bioscience), or corresponding isotype controls. Cells were fixed with 2% paraformaldehyde and 7-color analysis was performed using a BD FACSCanto II (BD Biosciences). Data was analyzed using BD FACS Diva software (BD Biosciences).

## Supplementary Material

Refer to Web version on PubMed Central for supplementary material.

## Acknowledgments

We thank Richard Reisdorph for technical assistance. Cara Wilson and Eric Lee for procurement of tissues for histological analysis. Work was supported by NIH Grants DK50189, DK09548, HL60569 and DK088663 and by a CCFA Career Development Award (to E.L.C.).

## References

- Amulic B, Cazalet C, Hayes GL, Metzler KD, Zychlinsky A. Neutrophil function: from mechanisms to disease. *Annual review of immunology*. 2012; 30:459–489.
- Beck PL, Ihara E, Hirota SA, MacDonald JA, Meng D, Nanthakumar NN, Podolsky DK, Xavier RJ. Exploring the interplay of barrier function and leukocyte recruitment in intestinal inflammation by targeting fucosyltransferase VII and trefoil factor 3. *American journal of physiology. Gastrointestinal and liver physiology*. 2010; 299:G43–53. [PubMed: 20299601]
- Bobrie A, Krumeich S, Reyat F, Recchi C, Moita LF, Seabra MC, Ostrowski M, Thery C. Rab27a supports exosome-dependent and -independent mechanisms that modify the tumor microenvironment and can promote tumor progression. *Cancer research*. 2012; 72:4920–4930. [PubMed: 22865453]
- Brinkmann V, Reichard U, Goosmann C, Fauler B, Uhlemann Y, Weiss DS, Weinrauch Y, Zychlinsky A. Neutrophil extracellular traps kill bacteria. *Science (New York, NY)*. 2004; 303:1532–1535.
- Campbell EL, MacManus CF, Kominsky DJ, Keely S, Glover LE, Bowers BE, Scully M, Bruyninckx WJ, Colgan SP. Resolvin E1-induced intestinal alkaline phosphatase promotes resolution of inflammation through LPS detoxification. *Proceedings of the National Academy of Sciences of the United States of America*. 2010; 107:14298–14303. [PubMed: 20660763]
- Chen LW, Egan L, Li ZW, Greten FR, Kagnoff MF, Karin M. The two faces of IKK and NF-kappaB inhibition: prevention of systemic inflammation but increased local injury following intestinal ischemia-reperfusion. *Nature medicine*. 2003; 9:575–581.
- Colgan SP, Curtis VF, Campbell EL. The Inflammatory Tissue Microenvironment in IBD. *Inflammatory bowel diseases*. 2013a; 19:2238–2244. [PubMed: 23702808]
- Colgan SP, Ehrentraut SF, Glover LE, Kominsky DJ, Campbell EL. Contributions of neutrophils to resolution of mucosal inflammation. *Immunologic research*. 2013b; 55:75–82. [PubMed: 22968707]
- Colgan SP, Taylor CT. Hypoxia: an alarm signal during intestinal inflammation. *Nature reviews*. 2010; 7:281–287.
- Cox G, Crossley J, Xing Z. Macrophage engulfment of apoptotic neutrophils contributes to the resolution of acute pulmonary inflammation in vivo. *American journal of respiratory cell and molecular biology*. 1995; 12:232–237. [PubMed: 7865221]
- Cross AR, Jones OT. The effect of the inhibitor diphenylene iodonium on the superoxide-generating system of neutrophils. Specific labelling of a component polypeptide of the oxidase. *The Biochemical journal*. 1986; 237:111–116. [PubMed: 3800872]
- Cross AR, Segal AW. The NADPH oxidase of professional phagocytes--prototype of the NOX electron transport chain systems. *Biochimica et biophysica acta*. 2004; 1657:1–22. [PubMed: 15238208]

- Cummins EP, Seeballuck F, Keely SJ, Mangan NE, Callanan JJ, Fallon PG, Taylor CT. The hydroxylase inhibitor dimethyloxalylglycine is protective in a murine model of colitis. *Gastroenterology*. 2008; 134:156–165. [PubMed: 18166353]
- Dalli J, Serhan CN. Specific lipid mediator signatures of human phagocytes: microparticles stimulate macrophage efferocytosis and pro-resolving mediators. *Blood*. 2012; 120:e60–72. [PubMed: 22904297]
- Dinauer MC, Orkin SH, Brown R, Jesaitis AJ, Parkos CA. The glycoprotein encoded by the X-linked chronic granulomatous disease locus is a component of the neutrophil cytochrome b complex. *Nature*. 1987; 327:717–720. [PubMed: 3600768]
- Ehrentraut SF, Kominsky DJ, Glover LE, Campbell EL, Kelly CJ, Bowers BE, Bayless AJ, Colgan SP. Central role for endothelial human deneddylase-1/SENp8 in fine-tuning the vascular inflammatory response. *J Immunol*. 2013; 190:392–400. [PubMed: 23209320]
- Furuta GT, Turner JR, Taylor CT, Hershberg RM, Comerford K, Narravula S, Podolsky DK, Colgan SP. Hypoxia-inducible factor 1-dependent induction of intestinal trefoil factor protects barrier function during hypoxia. *The Journal of experimental medicine*. 2001; 193:1027–1034. [PubMed: 11342587]
- Huang JS, Noack D, Rae J, Ellis BA, Newbury R, Pong AL, Lavine JE, Curnutte JT, Bastian J. Chronic granulomatous disease caused by a deficiency in p47(phox) mimicking Crohn's disease. *Clin Gastroenterol Hepatol*. 2004; 2:690–695. [PubMed: 15290662]
- Johansson ME, Larsson JM, Hansson GC. The two mucus layers of colon are organized by the MUC2 mucin, whereas the outer layer is a legislator of host-microbial interactions. *Proceedings of the National Academy of Sciences of the United States of America*. 2011; 108(Suppl 1):4659–4665. [PubMed: 20615996]
- Karhausen J, Furuta GT, Tomaszewski JE, Johnson RS, Colgan SP, Haase VH. Epithelial hypoxia-inducible factor-1 is protective in murine experimental colitis. *The Journal of clinical investigation*. 2004; 114:1098–1106. [PubMed: 15489957]
- Khor B, Gardet A, Xavier RJ. Genetics and pathogenesis of inflammatory bowel disease. *Nature*. 2011; 474:307–317. [PubMed: 21677747]
- Kominsky DJ, Campbell EL, Colgan SP. Metabolic shifts in immunity and inflammation. *J Immunol*. 2010; 184:4062–4068. [PubMed: 20368286]
- Kuhl AA, Kakirman H, Janotta M, Dreher S, Cremer P, Pawlowski NN, Loddenkemper C, Heimesaat MM, Grollich K, Zeitz M, et al. Aggravation of different types of experimental colitis by depletion or adhesion blockade of neutrophils. *Gastroenterology*. 2007; 133:1882–1892. [PubMed: 18054560]
- Lim K, Sumagin R, Hyun YM. Extravasating Neutrophil-derived Microparticles Preserve Vascular Barrier Function in Inflamed Tissue. *Immune network*. 2013; 13:102–106. [PubMed: 23885224]
- Louis NA, Hamilton KE, Canny G, Shekels LL, Ho SB, Colgan SP. Selective induction of mucin-3 by hypoxia in intestinal epithelia. *Journal of cellular biochemistry*. 2006; 99:1616–1627. [PubMed: 16823775]
- Mashimo H, Wu DC, Podolsky DK, Fishman MC. Impaired defense of intestinal mucosa in mice lacking intestinal trefoil factor. *Science (New York, NY)*. 1996; 274:262–265.
- Mittelbrunn M, Sanchez-Madrid F. Intercellular communication: diverse structures for exchange of genetic information. *Nature reviews Molecular cell biology*. 2012; 13:328–335.
- Nauseef WM. Biological roles for the NOX family NADPH oxidases. *The Journal of biological chemistry*. 2008; 283:16961–16965. [PubMed: 18420576]
- Okumura CY, Hollands A, Tran DN, Olson J, Dahesh S, von Kockritz-Blickwede M, Thienphrapa W, Corle C, Jeung SN, Kotsakis A, et al. A new pharmacological agent (AKB-4924) stabilizes hypoxia inducible factor-1 (HIF-1) and increases skin innate defenses against bacterial infection. *J Mol Med (Berl)*. 2012; 90:1079–1089. [PubMed: 22371073]
- Polosukhin VV, Cates JM, Lawson WE, Milstone AP, Matafonov AG, Massion PP, Lee JW, Randell SH, Blackwell TS. Hypoxia-inducible factor-1 signalling promotes goblet cell hyperplasia in airway epithelium. *The Journal of pathology*. 2011; 224:203–211. [PubMed: 21557221]

- Radi R, Beckman JS, Bush KM, Freeman BA. Peroxynitrite oxidation of sulfhydryls. The cytotoxic potential of superoxide and nitric oxide. *The Journal of biological chemistry*. 1991; 266:4244–4250. [PubMed: 1847917]
- Robinson A, Keely S, Karhausen J, Gerich ME, Furuta GT, Colgan SP. Mucosal protection by hypoxia-inducible factor prolyl hydroxylase inhibition. *Gastroenterology*. 2008; 134:145–155. [PubMed: 18166352]
- Safran M, Kim WY, O'Connell F, Flippin L, Gunzler V, Horner JW, Depinho RA, Kaelin WG Jr. Mouse model for noninvasive imaging of HIF prolyl hydroxylase activity: assessment of an oral agent that stimulates erythropoietin production. *Proceedings of the National Academy of Sciences of the United States of America*. 2006; 103:105–110. [PubMed: 16373502]
- Sanmun D, Witas E, Jitkaew S, Tyurina YY, Kagan VE, Ahlin A, Palmblad J, Fadeel B. Involvement of a functional NADPH oxidase in neutrophils and macrophages during programmed cell clearance: implications for chronic granulomatous disease. *American journal of physiology*. 2009; 297:C621–631. [PubMed: 19570889]
- Savill JS, Wyllie AH, Henson JE, Walport MJ, Henson PM, Haslett C. Macrophage phagocytosis of aging neutrophils in inflammation. Programmed cell death in the neutrophil leads to its recognition by macrophages. *The Journal of clinical investigation*. 1989; 83:865–875. [PubMed: 2921324]
- Serhan CN, Chiang N. Resolution phase lipid mediators of inflammation: agonists of resolution. *Current opinion in pharmacology*. 2013; 13:632–640. [PubMed: 23747022]
- Stie J, Jesaitis AJ. Reorganization of the human neutrophil plasma membrane is associated with functional priming: implications for neutrophil preparations. *Journal of leukocyte biology*. 2007; 81:672–685. [PubMed: 17170075]
- Taupin D, Podolsky DK. Trefoil factors: initiators of mucosal healing. *Nature reviews Molecular cell biology*. 2003; 4:721–732.
- Taupin DR, Kinoshita K, Podolsky DK. Intestinal trefoil factor confers colonic epithelial resistance to apoptosis. *Proceedings of the National Academy of Sciences of the United States of America*. 2000; 97:799–804. [PubMed: 10639160]
- Van der Sluis M, De Koning BA, De Bruijn AC, Velcich A, Meijerink JP, Van Goudoever JB, Buller HA, Dekker J, Van Seuningen I, Renes IB, Einerhand AW. Muc2-deficient mice spontaneously develop colitis, indicating that MUC2 is critical for colonic protection. *Gastroenterology*. 2006; 131:117–129. [PubMed: 16831596]
- Van Rees EP, Palmen MJ, Van De Goot FR, Macher BA, Dieleman LA. Leukocyte migration in experimental inflammatory bowel disease. *Mediators of inflammation*. 1997; 6:85–93. [PubMed: 18472841]
- Zen K, Parkos CA. Leukocyte-epithelial interactions. *Current opinion in cell biology*. 2003; 15:557–564. [PubMed: 14519390]



**Highlights**

- Infiltrating PMN consume sufficient O<sub>2</sub> to render adjacent colonic epithelia hypoxic
- Hypoxia reporter mice demonstrate PMN-dependent hypoxia in inflamed colitic lesions
- CGD mice do not incite mucosal hypoxia and develop severe non-resolving colitis
- Mucosal HIF stabilization ameliorates colitis severity in wild type and CGD mice

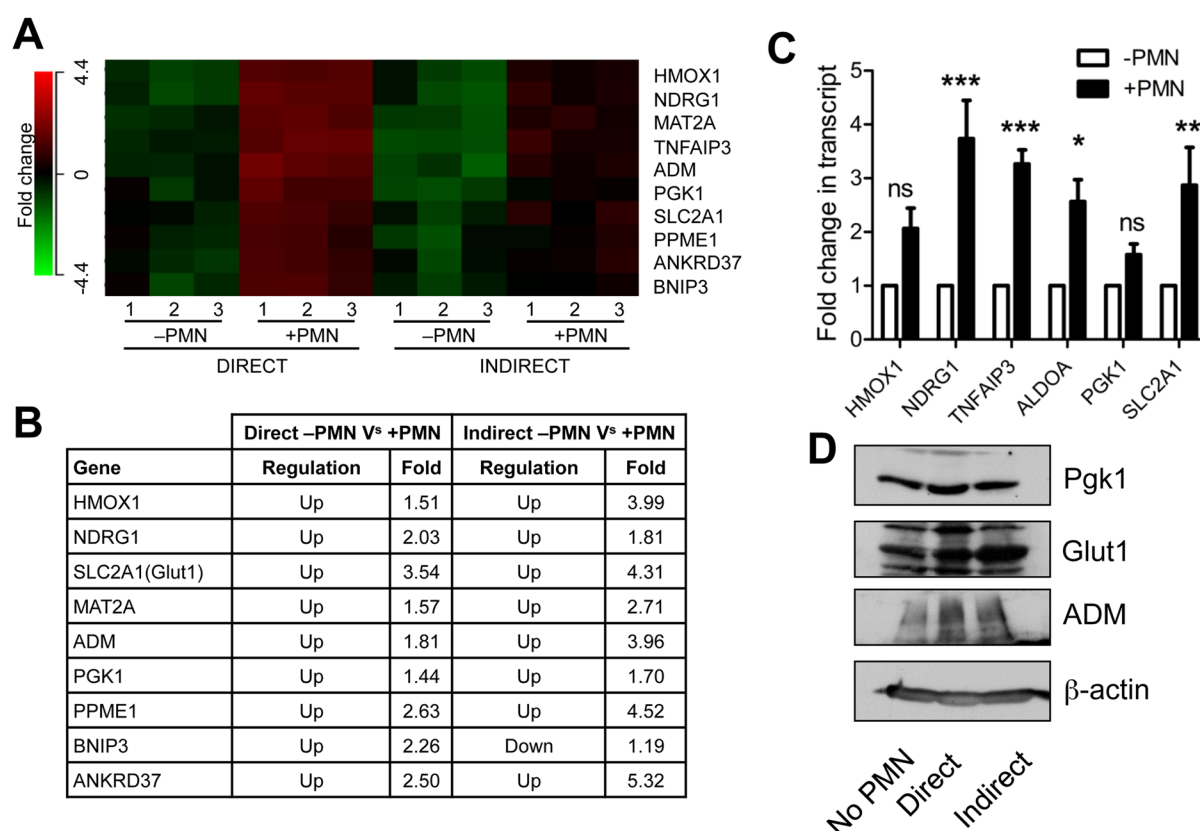


**Figure 1. Transmigrating neutrophils induce transcriptional imprinting in intestinal epithelial cells**

(A) Microarrays were hybridized with cDNA synthesized from epithelial RNA isolated from “Direct” versus “Indirect” transmigration experiments. Three separate experiments were performed and ( $n = 3$ ). (B) Table highlighting fold changes between groups. Statistical cutoff was set to  $P < 0.05$ . (C) Validation of hypoxia-responsive gene cluster by qPCR in the “Indirect” model. Values are means  $\pm$  SEM and are pooled from three independent experiments ( $n = 3$ ; \*,  $P < 0.05$ ; \*\*,  $P < 0.01$ ; \*\*\*,  $P < 0.001$ ; two-way ANOVA). (D) Validation of hypoxia-responsive target induction by immunoblotting for GLUT1, PGK1 and ADM.  $\beta$ -actin used as loading control. Images are representative of three independent experiments. See also Figure S1.

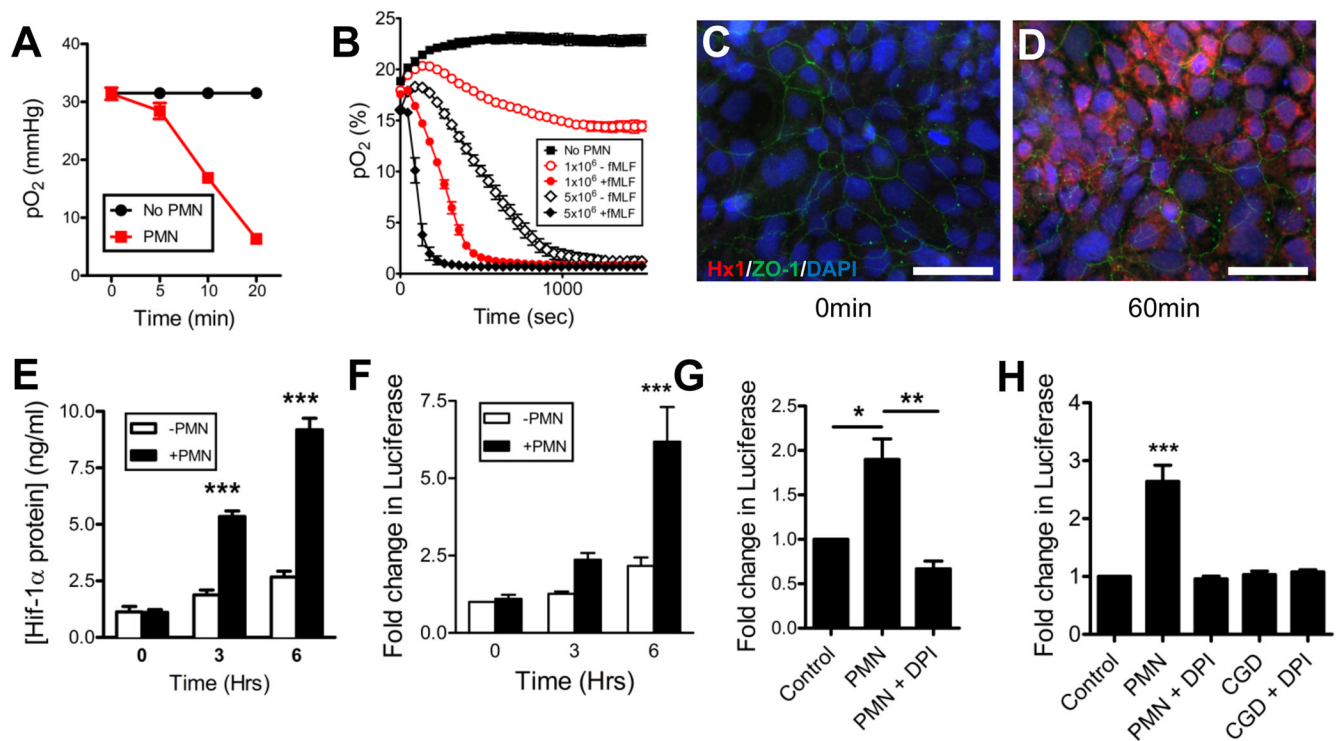


**Figure 2. Activated neutrophils rapidly deplete O<sub>2</sub> and induce HIF-1α stabilization via respiratory burst**

(A) pO<sub>2</sub> values were recorded in hypoxia chamber set to 4% O<sub>2</sub>, using a OxoProbe at indicated time points in the presence of 1×10<sup>6</sup> PMN, activated with fMLF. Data are representative of three independent experiments and presented as means ± SD ( $n = 3$ ;  $P < 0.001$ ; two-way ANOVA). (B) Consumption of dissolved O<sub>2</sub> in normoxia was monitored in real-time using OxoDishes mounted on an SDR O<sub>2</sub> sensor reader in the presence of increasing numbers of PMN ± activation with fMLF set up with the “SDR real-time O<sub>2</sub>” (see Figure S1d) model. Data is representative of three independent experiments and presented as means ± SD ( $n = 3$ ;  $P < 0.001$  throughout time course for ± PMN;  $P < 0.001$  throughout time course for 1×10<sup>6</sup> PMN ± chemoattractant;  $P < 0.001$  between 46 and 948 seconds for 5×10<sup>6</sup> PMN ± chemoattractant and  $P < 0.001$  between 46 and 407 seconds for 1×10<sup>6</sup> versus 5×10<sup>6</sup> with chemoattractant; two-way ANOVA). (C) Immunofluorescent staining of T84 IECs exposed to PMN using the “Co-culture” model (see Figure S1c) for 0min and (D) 60min, representative images from two independent experiments. Hypoxyprome-1 adduct staining (red), ZO-1 (green) and nuclei (blue). Scale bar = 200μm. (E) Nuclear accumulation of HIF-1α protein was assayed by Mesoscale ELISA, following exposure of epithelia to activated PMN by “Co-culture” model. Data are represented as means ± SEM and are pooled from three independent experiments ( $n = 3$ ;  $P < 0.001$  by two-way ANOVA). (F) IECs transfected with HRE-firefly and SV40-renilla Luciferase reporters and subsequently exposed to activated PMN, indicated increased HIF activity Data are represented as means ± SEM and are pooled from three independent experiments ( $n = 3$ ;  $P < 0.001$  by two-way ANOVA). (G) IECs transfected with HRE-firefly and SV40-renilla luciferase reporters and subsequently exposed to pre-treated PMN in the presence of fMLF. Data are represented as means ± SEM and are pooled from three independent experiments ( $n = 3$ ;  $P < 0.05$  for ± PMN;  $P < 0.01$  for PMN versus PMN+DPI; one-way ANOVA; DPI = diphenyleneiodonium). (H) HRE-transfected Caco-2 IECs, with subsequent exposure to activated PMN from wild-type or CGD mice. Data are represented as means ± SEM and are

pooled from three independent experiments ( $n = 3$ ;  $P < 0.001$  for no PMN versus wild-type PMN;  $P > 0.05$  for no PMN versus PMN+DPI;  $P > 0.05$  for no PMN versus CGD PMN; one-way ANOVA). See also Figure S2.

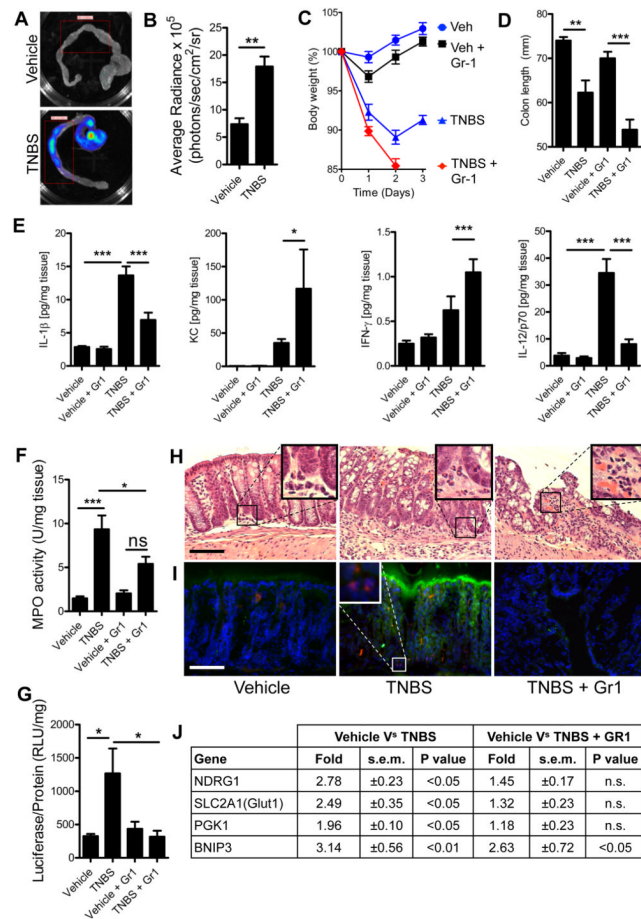


**Figure 3. Neutrophil accumulation in colitis induces “inflammatory hypoxia”**

(A) Representative image of colons excised from Vehicle and TNBS-treated ODD-Luc reporter mice, injected with D-Luciferin before sacrifice and imaged for luciferase activity. (B) Quantification of bioluminescent imaging values represent mean  $\pm$  SEM. ( $n = 5$ ; \*\*,  $P < 0.01$ ; two-tailed Student's  $t$ -test). Gr-1 antibody was used to deplete PMN in ODD-Luc mice, prior to induction of colitis with TNBS. PMN-depleted ODD-Luc mice developed more severe colitis than sham injected mice, demonstrated by (C) weight-loss curves ( $P < 0.001$  for Vehicle versus TNBS;  $P < 0.001$  TNBS versus TNBS+Gr-1; two-way ANOVA) and (D) colon length ( $P > 0.05$  for Vehicle versus TNBS;  $P < 0.05$  for Vehicle+Gr-1 versus TNBS+Gr-1; one-way ANOVA). Data are represented as means  $\pm$  SEM and are pooled from three independent experiments ( $n = 12$ ). (E) Protein lysates were profiled for cytokines and normalized to total protein (\*,  $P < 0.05$ ; \*\*\*,  $P < 0.001$ ; one-way ANOVA). (F) MPO activity in tissues post-TNBS  $\pm$  Gr-1. Data are represented as means  $\pm$  SEM and are pooled from three independent experiments ( $n = 12$ ). (G) Tissue homogenates from distal colons of TNBS-treated mice  $\pm$  Gr-1 depletion revealed an increase in luciferase activity in TNBS-treated mice ( $P < 0.05$ ), which was attenuated by Gr-1 depletion ( $P < 0.05$ ; one-way ANOVA). Data represented as means  $\pm$  SEM and pooled from two independent experiments ( $n = 8$ ). (H) Representative H&E stained sections revealed PMN accumulation in TNBS, which was attenuated by Gr-1. Inset highlights typical infiltrate observed. (I) IHC for Luciferase and Ly6g indicated accumulation of PMN in TNBS (highlighted in inset), which coincided with hypoxic Luciferase accumulation and an abrogation of both with Gr-1 depletion. Scale bars = 100 $\mu$ m. (J) Fold increases in HIF target gene transcript expression in



TNBS  $\pm$  Gr-1 measured by qPCR, data represents means  $\pm$  SEM and are pooled from three independent experiments ( $n = 12$ ). See also Figure S3.

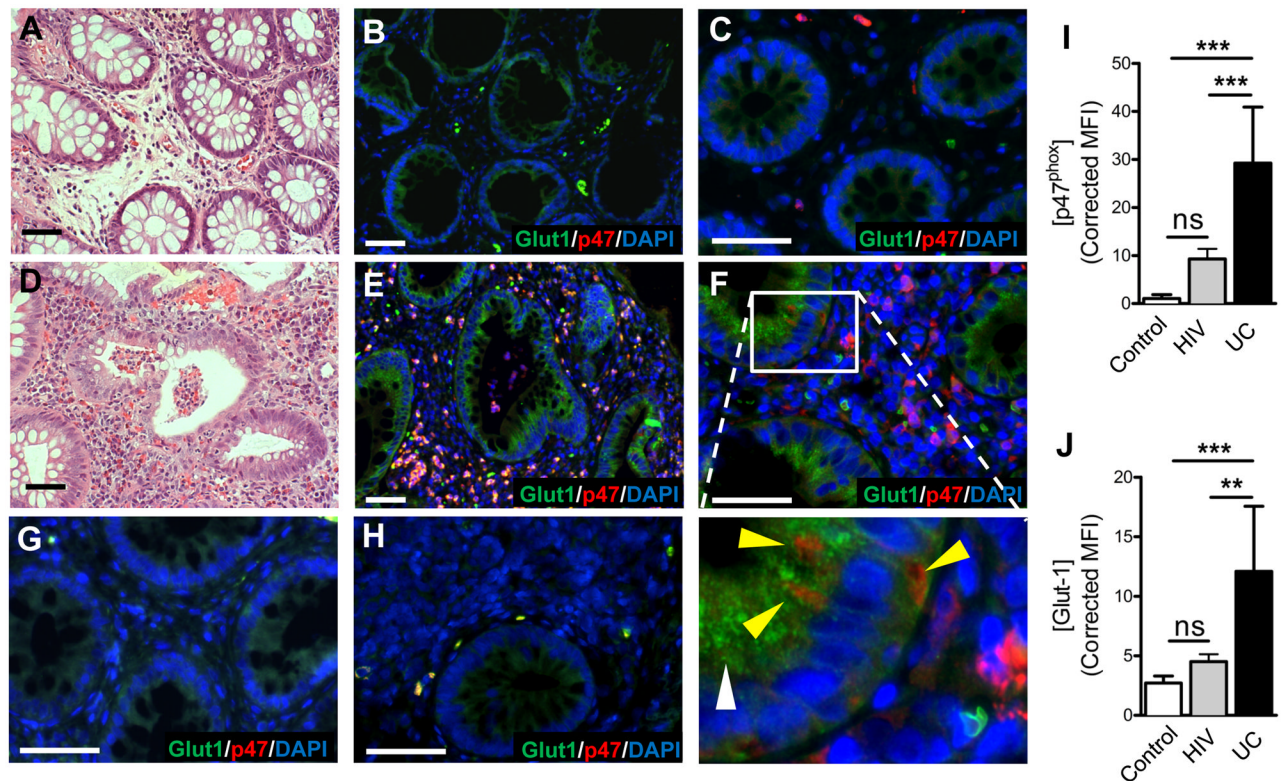


**Figure 4. Ulcerative colitis patients with crypt abscesses demonstrate hypoxia-dependent target induction**

Biopsies from (A, B, C) uninfamed margins and (D, E, F) inflamed regions with active crypt abscess formation in patients with ulcerative colitis, were processed for H&E (A, D) and stained for hypoxia-responsive Glut-1 (green), neutrophil p47<sup>phox</sup> (red) and nuclei (blue). Higher magnification of uninfamed tissue (C) or colitis (F) indicates de novo Glut1 (white arrowhead) adjacent to transmigrating PMN (yellow arrowhead). Disease controls from un-infamed (G) and HIV patient (H) biopsies. Quantification of staining intensities for p47 (G) and Glut1 (H). Measurements were made from 5 ROIs per slide and 5 slides per group. Data represent means  $\pm$  SEM ( $n = 25$ ). (\*\*,  $P < 0.01$ ; \*\*\*,  $P < 0.001$ ; one-way ANOVA). Scale bars = 50 $\mu$ m.

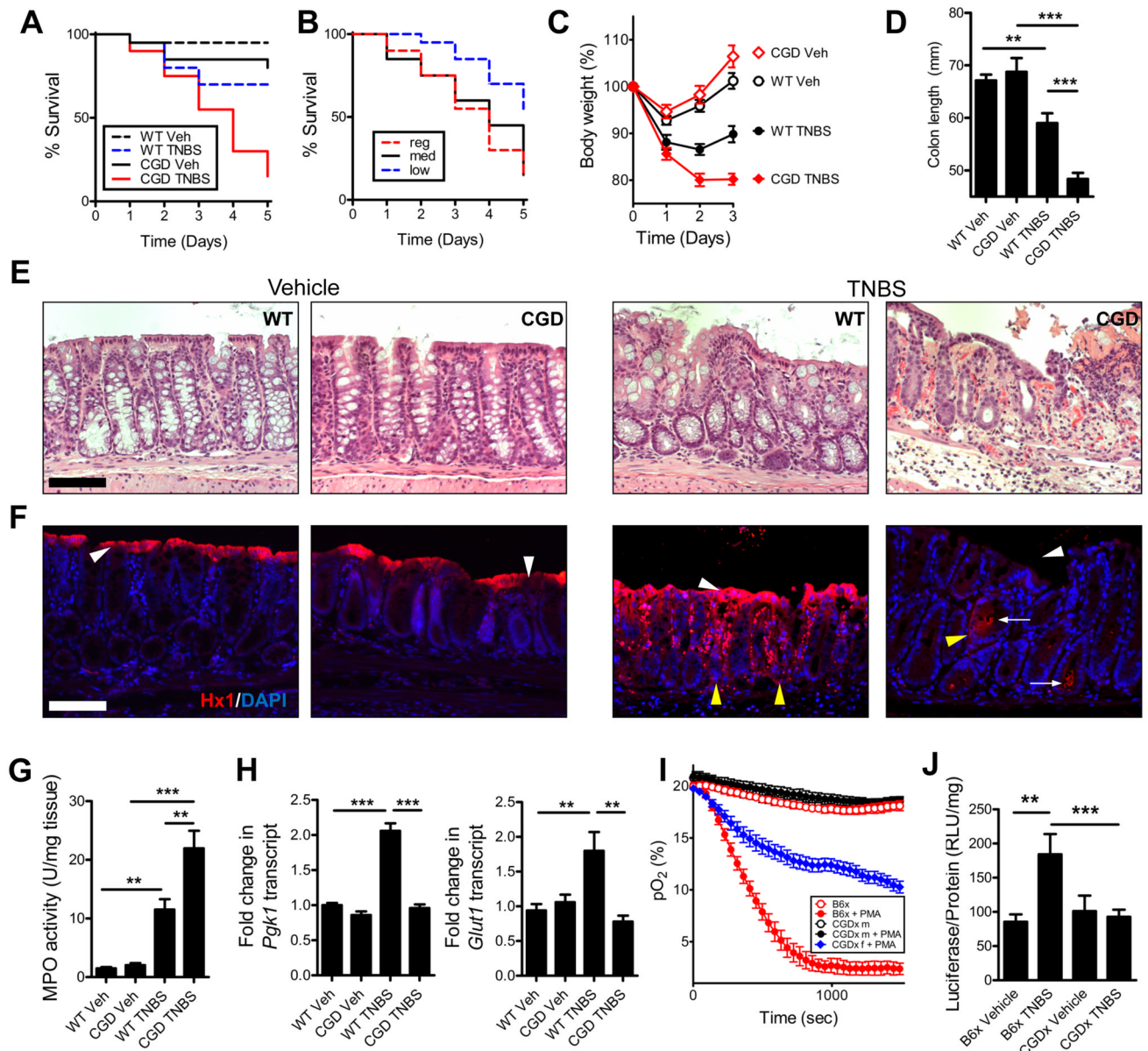


**Figure 5. Neutrophil respiratory burst-deficient (CGD) mice develop severe non-resolving colitis** (A) Survival curves for C57/B6 versus CGD following TNBS administration ( $P < 0.001$  compared with vehicle;  $P < 0.05$  compared with wild-type TNBS; Gehan-Breslow-Wilcoxon test). Data represents means  $\pm$  SEM ( $n = 6$ ). (B) Survival curves for CGD mice on *regular* (2.5% TNBS in 50% EtOH), *medium* (2% TNBS in 45% EtOH) and *low* TNBS regimen (2% TNBS in 40% EtOH). Data represents means  $\pm$  SEM ( $n = 6$ ) ( $P < 0.005$  low compared with regular dose;  $P < 0.05$  low compared with medium dose TNBS; Gehan-Breslow-Wilcoxon test). (C) Weight-loss curves and (D) colon lengths of CGD mice on low TNBS regimen indicated a defect in resolution. Data are represented as means  $\pm$  SEM and are pooled from three independent experiments ( $n = 8-12$ ). (E) Representative H&E stained sections revealed severe PMN accumulation in CGD mice treated with TNBS. (F) Hypoxyprobe (red) staining and nuclear (blue) counterstain of wild type versus CGD mice  $\pm$  TNBS. White arrowheads indicate presence/absence of luminal epithelial cells; yellow

arrowheads indicate crypts. Arrows indicate potential presence of bacteria. Scale bars = 100 $\mu$ m. **(G)** Myeloperoxidase activity assay indicated increased PMN in TNBS (\*\*,  $P < 0.01$ ; \*\*\*,  $P < 0.001$ ; one-way ANOVA). Data are represented as means  $\pm$  SEM and are pooled from three independent experiments ( $n = 8-12$ ). **(H)** Hypoxia target gene expression from purified colonic epithelial cells for *Pgk1* and *Glut1* in TNBS. Data are represented as means  $\pm$  SEM (\*\*,  $P < 0.01$ ; \*\*\*,  $P < 0.001$ ; one-way ANOVA). **(I)** O<sub>2</sub> consumption of B6x versus CGDx m (male) and f (female) ( $P < 0.001$  B6x  $\pm$  PMA;  $P > 0.05$  male CGDx  $\pm$  PMA;  $P < 0.001$  female CGDx versus B6x – PMA;  $P < 0.001$  female CGDx versus B6x +PMA; two-way ANOVA). Data is representative of three independent experiments and presented as means  $\pm$  SD ( $n = 6$ ). **(J)** Tissue luciferase was assayed following a low TNBS regimen in both B6x ( $P < 0.01$  Vehicle versus TNBS in B6x) and CGDx ( $P > 0.05$  CGDx vehicle versus TNBS;  $P < 0.05$  for B6x TNBS versus CGDx TNBS; one-way ANOVA). Data represented as means  $\pm$  SEM and are pooled from two independent experiments ( $n = 8$ ). See also Figure S4.



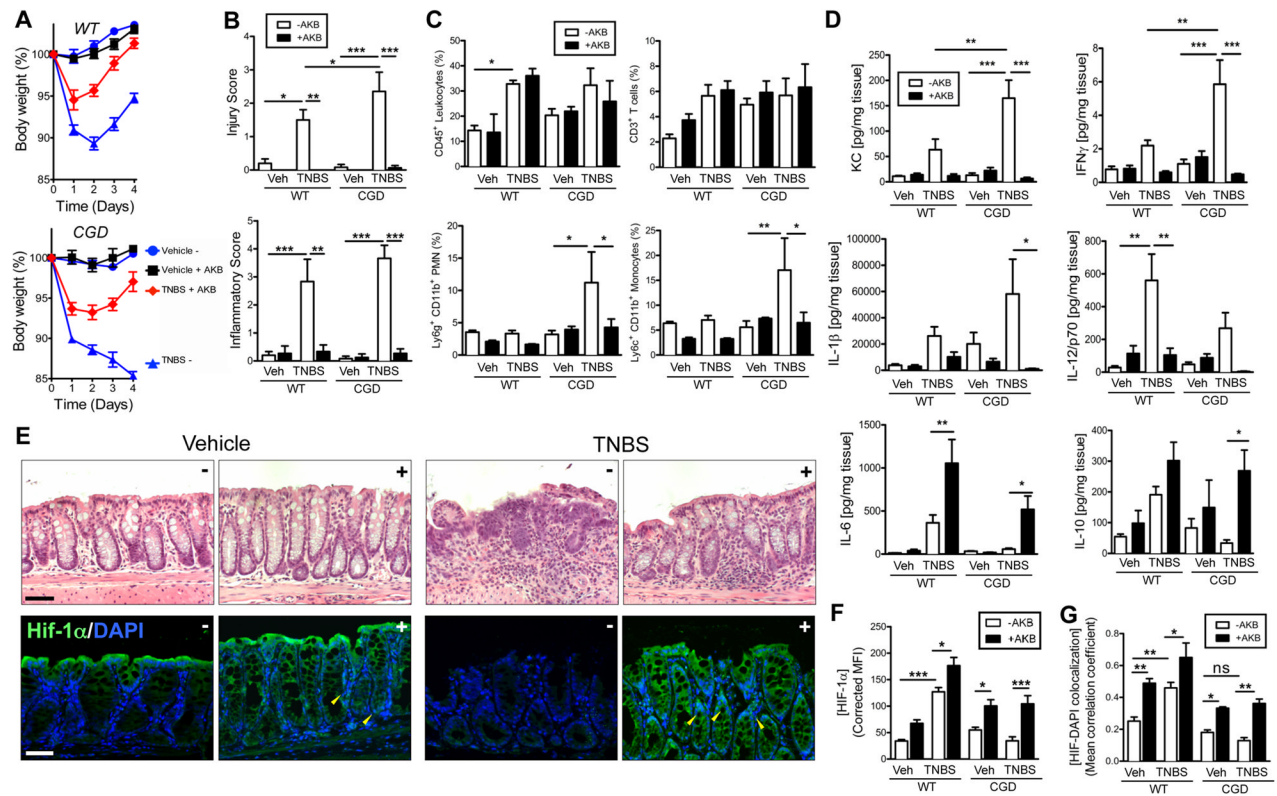


**Figure 6. Pharmacological intervention with prolyl hydroxylase inhibitor rectifies resolution defect in CGD mice**

Wild type and CGD mice treated with AKB-4924 or vehicle on days -1 through 2 and TNBS or vehicle was administered on day 0. Weight loss curves for (A) wild type ( $P < 0.001$  for vehicle versus TNBS on days 1–3;  $P < 0.001$  TNBS versus TNBS+ AKB-4924 on days 2–3;  $P > 0.05$  TNBS+AKB-4924 versus Vehicle+ AKB-4924 on days 2–3) and CGD mice ( $P < 0.001$  CGD vehicle versus CGD TNBS on days 1–3; two-way ANOVA). Data are represented as means  $\pm$  SEM and are pooled from three independent experiments ( $n = 8–12$ ). (B) Histological scoring (Inflammatory score left panel; Injury score right panel) of colon sections ( $n = 4–6$ ; \*,  $P < 0.05$ ; \*\*,  $P < 0.01$ ; \*\*\*,  $P < 0.001$ ; one-way ANOVA). (C) Flow cytometric analysis of infiltrating leukocytes: CD45<sup>+</sup> (bulk leukocytes), CD3<sup>+</sup> (T-cells), Ly6g<sup>+</sup>CD11b<sup>+</sup> (neutrophils) and Ly6c<sup>+</sup>CD11b<sup>+</sup> (monocytes). (\*,  $P < 0.05$ ; \*\*,  $P < 0.01$ ; two-way ANOVA). Data are representative of two independent experiments and presented as means  $\pm$  SD ( $n = 4–6$  mice per group) ( $p < 0.01$  by one-way ANOVA). (D) Tissue ELISAs for cytokines from wild type and CGD mice treated with AKB-4924  $\pm$  TNBS (\*,  $P < 0.05$ ; \*\*,  $P < 0.01$ ; \*\*\*,  $P < 0.001$ ; one-way ANOVA). Data are represented as means  $\pm$  SEM and are pooled from three independent experiments ( $n = 8–12$ ). (E) Representative H&E stained sections (top panels) from CGD mice with (+) or without (-) AKB-4924 and IHC staining (bottom panels) for HIF-1 $\alpha$  (green) and nuclei (blue). Scale bars = 100 $\mu$ m. Yellow arrowheads indicate co-localization in TNBS and AKB-4924-treated crypt epithelial cells. (F) Quantification of staining intensities for HIF-1 $\alpha$  and (G) co-localization analysis of HIF-1 $\alpha$  with nuclear DAPI. Data are represented as means  $\pm$  SEM of three pooled experiments ( $n = 8–12$ ), (\*,  $P < 0.05$ ; \*\*,  $P < 0.01$ ; \*\*\*,  $P < 0.001$ ; one-way ANOVA). See also Figure S5 and S6.



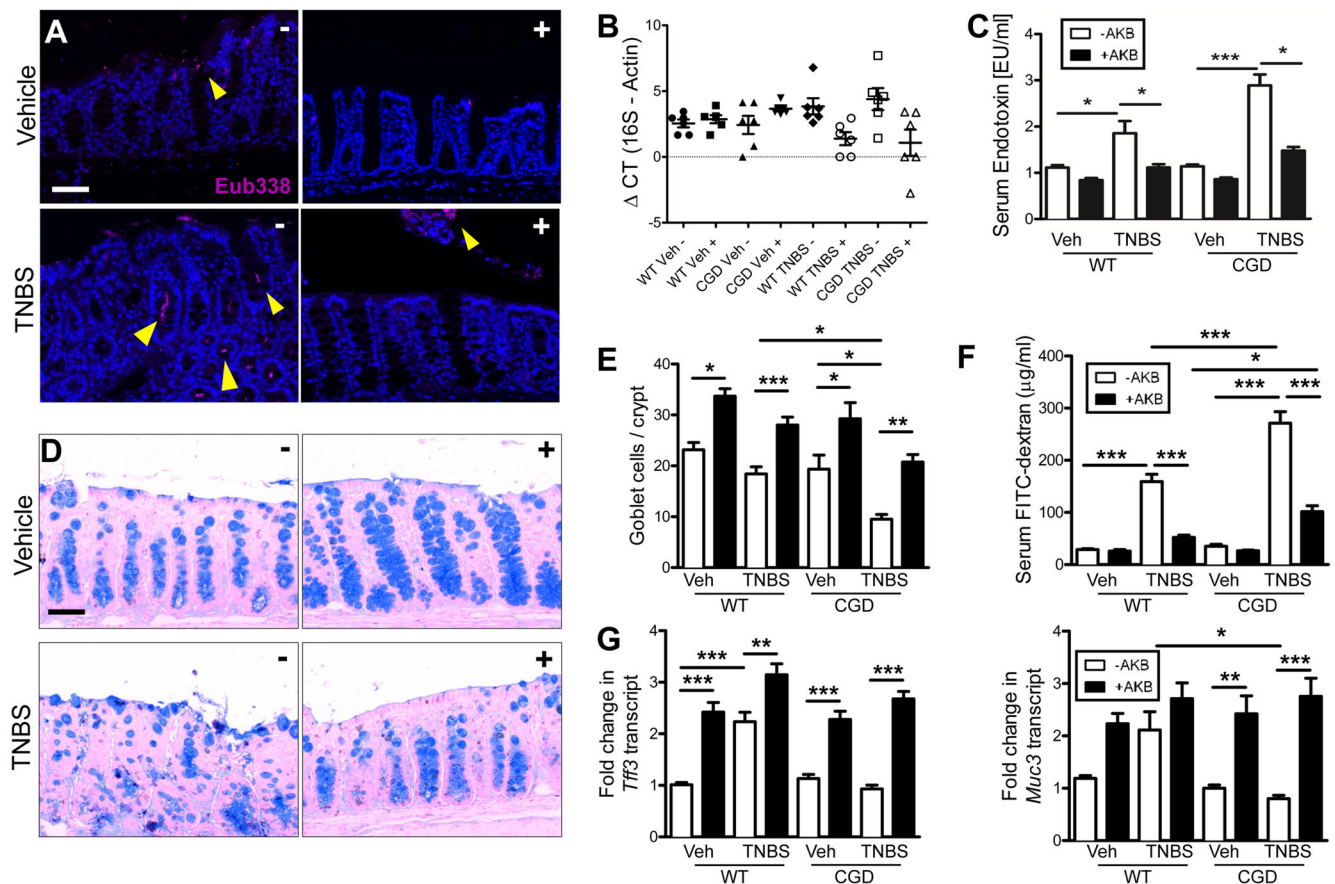


**Figure 7. HIF stabilization promotes mucosal protection against luminal bacteria in CGD mice via goblet cell function**

CGD mice treated with AKB-4924 or vehicle on days -1 through 2 and TNBS or vehicle was administered on day 0. Fluorescent in situ hybridization (FISH) was performed using Eub338 probe (magenta) in CGD mice (A) representative images indicated crypt infiltration of bacteria during colitis. (B) Quantification of bacterial dissemination to mesenteric lymph nodes was achieved by 16S rDNA qPCR. Data is presented as means ± SEM (n = 6). (C) Serum LPS quantification was measured by LAL assay. Data are represented as means ± SEM of three pooled experiments (n = 8–12). (D) Representative Alcian blue staining for goblet cells from CGD mice. (E) Quantification of goblet cell number per crypt in CGD mice. (F) GI permeability was assessed by measuring serum FITC 4hrs post gavage. Data is represented as mean ± SEM of three pooled experiments (n = 8–12). (G) Real-time qPCR of mucosal epithelial hypoxia target genes involved in regulating mucus barrier *Tff3* and *Muc3*. Data are represented as means ± SEM of three pooled experiments (n = 8–12), (\*,  $P < 0.05$ ; \*\*,  $P < 0.01$ ; \*\*\*,  $P < 0.001$ ; one-way ANOVA). See also Figure 7.